Unconventional Magnetic and Resistive Hysteresis in an Iodine-Bonded Molecular Conductor**

Genta Kawaguchi,[a] Mitsuhiko Maesato,*[,a] Tokutaro Komatsu,[a] Hiroshi Kitagawa,[a,b] Tatsuro Imakubo,[c] Andhika Kiswandhi,[d,e] David Graf,[d] and James S. Brooks[d]

In memory of James S. Brooks

Abstract: Simultaneous manipulation of both spin and charge is a crucial issue in magnetic conductors. We report on a strong correlation between magnetism and conductivity in the iodine-bonded molecular conductor $(DIETSe)_2FeBr_2Cl_2$ [DIETSe = diiodo(ethylenedithio)tetraselenafulvalene], which is the first molecular conductor showing a large hysteresis in both magnetic moment and magnetoresistance associated with a spin-flop transition. Utilizing a mixed-anion approach and iodine bonding interactions, we tailored a molecular conductor with random exchange interactions exhibiting unforeseen physical properties.

The discovery of giant magnetoresistance (GMR) in alternating ferromagnetic and nonmagnetic metal layers[1] has opened the door of spintronics.[2] Compared to the top down approach in inorganics, molecular materials have advantages in bottom up and low cost fabrication as well as diverse material design. Although molecular materials normally show weak interactions, when competing interactions are delicately balanced, small perturbations can give rise to a giant response.[3] Some π–*d* hybrid molecular conductors indeed show interesting spin–charge-coupled phenomena,[4] such as GMR[4a] and field-induced superconductivity.[4b]

Multi-instability or switching function is also an important issue in magnetic conductors. Quasi-one-dimensional (Q1D) π–*d* conductors[5–8] are good candidates having such properties because Q1D metals are susceptible to external stimuli due to low-dimensional instability. Recently, we found spin-flop switching and memory in $(DIETSe)_2FeCl_4$, where DIETSe denotes diiodo(ethylenedithio)tetraselenafulvalene (Figure 1a).[7] However, the hysteresis was only observed in resistance.

To introduce large hysteresis in both magnetism and conductivity, we propose to use a mixed-anion material, in which magnetic anions are mixed in a radical cation salt to induce random exchange interaction.

Herein we report on the discovery of large hysteresis in both magnetism and magnetoresistance (MR) associated with a spin-flop transition in a mixed-anion π–*d* conductor $(DIETSe)_2FeBr_2Cl_2$ (**1**). In contrast to inorganics, molecular materials have difficulties in alloying or chemical doping, while maintaining its crystal structure. It is because of weak intermolecular interactions, such as van der Waals interaction. By using iodine bonds,[6,9] however, we succeeded in fabricating the isostructural mixed-anion salts. This method allowed us to fine-tune π–*d* interactions and low-dimensional instability of itinerant π-electrons in Q1D π–*d* systems.

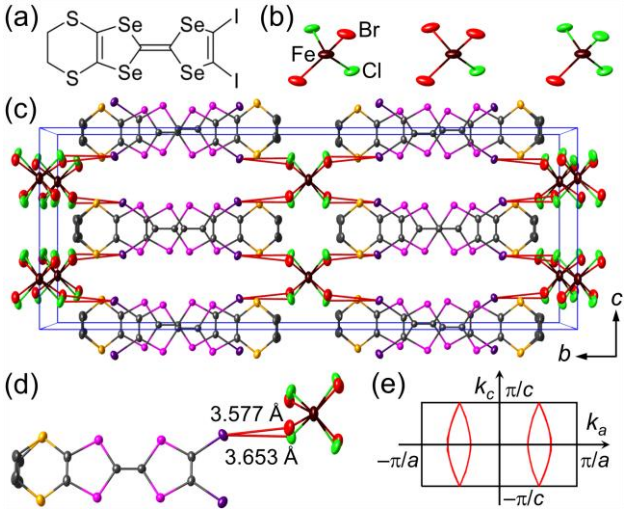

Figure 1. a) Molecular structure of DIETSe. b) Anions in a crystal of **1**. c) Crystal structure of **1** viewed along the *a*-axis. C, I, Se, S, Fe, Br, and Cl atoms are shown in gray, violet, pink, yellow, brown, red, and green, respectively, by a thermal ellipsoid model (50% probability). The site occupancy factors of Br and Cl are 0.5. Red lines show iodine bonds. d) Short contacts due to iodine bonds. e) Fermi surfaces of **1** in the k_c–k_a plane.

The DIETSe molecule was synthesized as described in the literature.[10] Single crystals of **1** and $(DIETSe)_2GaBr_2Cl_2$ (**2**) were prepared by an electrolytic method using supporting electrolytes of equimolar TBA-MBr_4 and TBA-MCl_4 [TBA = tetra-*n*-butylammonium; M = Fe, Ga]. The Br/Cl ratio was confirmed to be the same with synthetic ratio from energy-dispersive X-ray (EDX) analysis (Table S1 in the Supporting Information (SI)). We

[a] G. Kawaguchi, Prof. Dr. M. Maesato, Dr. T. Komatsu, Prof. Dr. H. Kitagawa
Division of Chemistry, Graduate School of Science
Kyoto University, Sakyo-ku, Kyoto 606-8502 (Japan)
E-mail: maesato@kuchem.kyoto-u.ac.jp
[b] JST-CREST, Goban-cho 7, Chiyoda-ku, Tokyo 102-0075 (Japan)
[c] Prof. Dr. T. Imakubo
Department of Materials Science and Technology
Nagaoka University of Technology
1603-1 Kamitomioka, Nagaoka, Niigata 940-2188 (Japan)
[d] Dr. A. Kiswandhi, Dr. D. Graf, Prof. Dr. J. S. Brooks[†]
National High Magnetic Field Laboratory, Florida State University,
1800 E. Paul Dirac Dr. Tallahassee, FL 32310-3706 (USA)
[e] Present address: Department of Physics, University of Texas at Dallas, 800 W. Campbell Rd., Richardson, TX 75080-3021 (USA)
[†] Deceased on September 27, 2014.
[**] The work was supported in part by Grants-in-Aid for JSPS Fellows (25-1778), Scientific Research (C) (25400367), (C) (25410090), (S) (23225005) from JSPS, and NSF-DMR 1157490, 1309146, the State of Florida, and the US DOE. The calculations and modellings were performed on the supercomputer of ACCMS, Kyoto University and SuperComputer System, Institute for Chemical Research, Kyoto University.

Supporting information for this article is available on the WWW under http://dx.doi.org/10.1002/anie.201503824.

note that, as shown in Figure 1b, several halogen-mixed anion species $MBr_xCl_{4-x}^-$ [M = Fe, Ga; x = 0, 1, 2, 3, 4] with majority of averaged-formula species are considered to coexist in a crystal with random orientation because such coexistence has been observed in $GaCl_4^-/GaBr_4^-$ mixture solution by the ^{71}Ga nuclear magnetic resonance (NMR) study.[11]

The crystal structures of **1** and **2** are isostructural to the pristine $(DIETSe)_2MX_4$ [M = Fe, Ga; X = Br, Cl] (Figures 1c, S1, S2).[6,12] DIETSe molecules uniformly stack parallel to the *a*-axis in a head-to-tail manner, giving rise to the highest conductivity along the *a*-axis direction. Figure 1d shows short I···X [X = Br, Cl] contacts between DIETSe and anion, which are shorter than the sum of the van der Waals radii: I···Cl = 3.73 Å, I···Br = 3.83 Å, indicating that the iodine bonds play an important role in stabilizing the structure.[6,9] The MBr_2Cl_2 [M = Fe, Ga] salts have nearly the same lattice parameters (Table S2). The Ga^{3+} ion is nonmagnetic (S = 0), while the Fe^{3+} ion has localized *d*-spins (S = 5/2). Therefore, **2** is a good reference with which to extract the nature of itinerant π-electrons. The band structures and Fermi surfaces of **1** and **2** were calculated based on the density-functional theory (Figure 1e, details in SI), indicating a Q1D electronic structure.

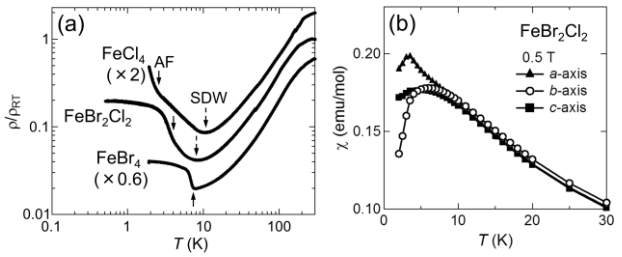

Figure 2. a) Electrical resistivity along the *b*-axis of the $FeCl_4$ salt, **1**, and $FeBr_4$ salt, normalized by the value at 300 K. For clarity, the values of the $FeCl_4$ and $FeBr_4$ salts are multiplied by 2 and 0.6, respectively. Broken and solid arrows show SDW and AF transitions, respectively. b) Magnetic susceptibility of **1** at 0.5 T along the *a*- (filled triangles), *b*- (open circles), and *c*-axes (filled squares).

The temperature dependent resistivities of **1** and the pristine FeX_4 [X = Br, Cl] salts are shown in Figure 2a. As shown by dashed arrows, the $FeCl_4$ salt and **1** undergo a metal–insulator (M–I) transition at 11 and 8 K, respectively. The similar M–I transition occurs in the $GaCl_4$ salt and **2** at 12 and 9 K, respectively (Figure S3). These are attributed to a spin-density-wave (SDW) transition from nesting instability of the Q1D Fermi surfaces. The previous ^{77}Se NMR study has confirmed an incommensurate SDW formation in the $GaCl_4$ salt.[13] In contrast, the $GaBr_4$ salt is metallic down to 1.9 K (Figure S3). These results indicate Br substitution suppresses the SDW transition to lower temperatures owing to an increase in the warping of Fermi surfaces. Besides the SDW transition, an additional steep increase in the resistivity, which is absent in the nonmagnetic Ga salts, appears at 2.5, 4, and 7 K in the $FeCl_4$ salt, **1**, and $FeBr_4$ salt, respectively (solid arrows). These anomalies correspond to antiferromagnetic (AF) transitions of *d*-spins, as discussed below.[6,7] The Néel temperature T_N increases with Br content, indicating systematic control of π–*d* interactions by anion mixing.

Figures 2b and S4 show the temperature dependence of the magnetic susceptibility χ of **1** along each crystallographic axis. Above 20 K, χ is well fitted by the Curie–Weiss law with Curie constant C = 4.5 emu K/mol and Weiss temperature θ = –14 K (Figure S4). Below 4 K, χ decreases with lowering temperature in an anisotropic nature, indicating long-range AF ordering with a magnetic easy axis along the *b*-axis. Since the value of T_N = 4 K agrees well with the resistivity anomaly (Figure 2a), the steep increase in resistance at T_N implies an AF ordering-induced charge gap. Assuming that the up- and down-spins of Fe^{3+} alternately order along the *a*-axis by an AF transition, $2k_F$ (= π/*a*) periodic modulation of the local moments appears, which can induce charge gap opening via strong π–*d* interactions.

To explore the magnetic-field effects on the electronic states, we employed a magnetic torque technique (details in SI). Figure 3a shows the magnetic torque τ divided by the field strength up to 35 T along the *b*-axis. Below 2 K, a sharp increase in τ/*H* appears around 2 T, attributed to spin-flop transitions of *d*-spins. Anomalies are also observed around 7 T below T_N, indicating AF boundaries, which are plotted as filled diamonds in temperature–magnetic field (*T*–*H*) phase diagram (Figure 4). In addition, τ/*H* shows a maximum above 15 T, and with increasing temperature, it shifts to higher fields, suggesting the saturation field H_{FM} (filled squares in Figure 4). This is also supported by the magnetization *M* measured at 2 K using a superconducting quantum interference device (SQUID) magnetometer: the linear extrapolation of *M* reaches 5 μ_B at about 13 T, which is comparable to H_{FM} (15 T) (Figure 3a). The obtained H_{FM} is almost intermediate between that of the $FeCl_4$ (6 T)[7] and $FeBr_4$ salts (22 T; also see Figure S5).[8] A wide gap is observed between the AF boundary and saturation field in **1**. This indicates no long-range order but a short-range order or fluctuations in the intermediate paramagnetic (PM) region, which is pronounced by anion mixing.

We discovered unconventional magnetic hysteresis at very low temperatures (< 1 K) by SQUID with a ^{3}He cryostat. Figure 3b displays a clear large hysteresis in magnetization *M* at 0.5 K, associated with a spin-flop transition (also see Figure S6). We also observed a similar hysteresis in magnetic torque at 0.3 K (Figure S5). The down-sweep magnetization, M_{down}, is significantly larger than the up-sweep one, M_{up} (Figure 3b). The field-induced state is found to be metastable, and the hysteresis disappears on subsequent heating. Figure 3c shows the temperature dependence of *M* at 1 T for the zero field cooled (ZFC) (open squares) and M_{down} (filled squares) after the field sweep at 0.5 K, whose initial points are equivalent to the emphasized squares in Figure 3b (also see SI). M_{down} decreases with increasing temperature and follows ZFC above 1.3 K, which is well reproduced by two different samples (Figure S7). These results indicate the hysteresis emerges only below 1.3 K.

Remarkably, the anomalous hysteresis also appears in the resistivity. Figure 5 shows MR of **1** under the magnetic field along the *b*-axis. Below T_N (4 K), the MR shows large anomalies with hysteresis, in sharp contrast to the monotonic MR in **2** (Figure S8). The former clearly demonstrates significant π–*d* interactions between itinerant π-electrons and AF *d*-spins. The dip structure in MR at 1.4 T and 2 K is attributed to a spin-flop transition of *d*-spins, which is confirmed by magnetic torque and magnetization (Figure S9). Furthermore, below 1.3 K the dip

position shifts to higher and lower fields for up- and down-sweeps, respectively, as indicated by the broken arrows in Figure 5 and filled (up-) and open (down-sweep) triangles in *T*–*H* phase diagram (Figure 4). The shaded region in Figure 4 is in good accordance with the magnetic hysteresis. In fact, the low-temperature hysteretic behaviors of MR, magnetization, and magnetic torque are well correlated (Figure S10). At higher magnetic fields, a negative MR is observed. As denoted by filled (up-) and open (down-sweep) circles in *T*–*H* phase diagram (Figure 4), the broad minimum in MR around 6 T corresponds to the AF boundary, in good agreement with the torque results.

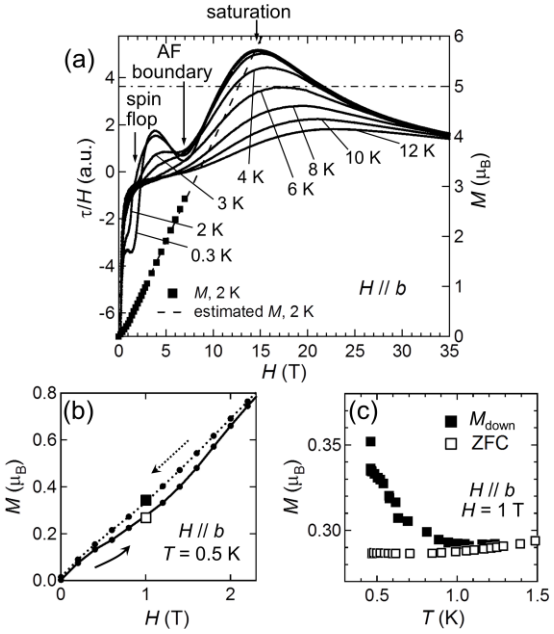

Figure 3. Magnetic torque and magnetization of **1** under magnetic field along the *b*-axis. a) Magnetic field dependence of torque divided by magnetic field, τ/H (left axis) and extrapolated magnetization (right axis). b) Magnetic field dependence of magnetization *M* at 0.5 K. Solid and dotted curves indicate *M* for up- and down-sweeps, respectively. c) Temperature dependence of *M* at 1 T. Open and filled squares denote ZFC and M_{down}, heating after field sweeping up to 5 T, respectively. Enlarged open and filled squares in Figure 3b correspond to the initial points of ZFC and M_{down} in Figure 3c, respectively.

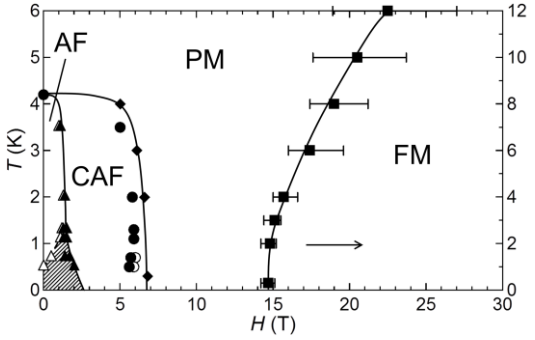

Figure 4. Temperature–magnetic field phase diagram of **1**. AF: antiferromagnetic, CAF: canted AF, PM: paramagnetic, FM: ferromagnetic. Filled diamonds show magnetic torque minimum. Filled squares represent maximum of torque (right axis). Filled and open triangles represent dip structures in up- and down-sweep magnetoresistance (MR, see Figure 5), respectively. Filled and open circles denote up- and down-sweep MR minimum, respectively. The shaded region shows hysteresis.

The large hysteresis in *M* and the cusp in χ along the *a*-axis at T_N (Figure 2b) are reminiscent of weak ferromagnetism from spin canting.[14] However, the hysteresis is negligible near to zero field, in contrast to typical canted AF (CAF) systems.[15] Instead, *M* shows a large hysteresis around the spin-flop field (Figure 3b). Spin flop is a first-order transition, and therefore, involves hysteresis. However, the hysteresis is normally very small, as seen in the pristine FeX_4 [X = Br, Cl] salts (Figure S5). On the other hand, **1** shows an extraordinarily large hysteresis around spin-flop field below 1.3 K. These results suggest that anion mixing plays a key role in the hysteresis phenomena. The randomly substituted halide ions (Cl or Br) induce random magnetic interactions. The so-called random exchange effect can in part account for the enhancement of the hysteresis at spin-flop field, as discussed for some inorganic alloys.[16] The less pronounced spin-flop transition in down-sweep *M* implies continuous changes in the domain ratio of coexisting AF and CAF phases. In contrast to a homogeneous system, a number of pinning centers may be present in the mixed halide system, giving rise to a significant effect on the domain wall dynamics.

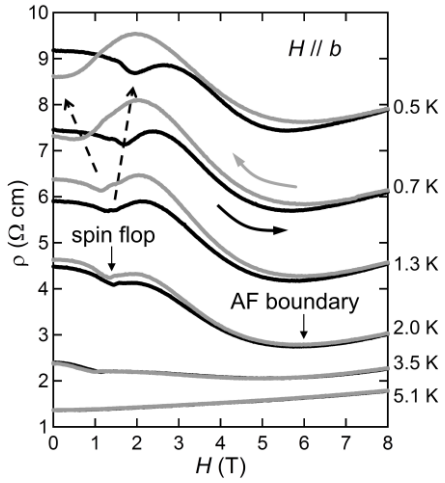

Figure 5. Magnetoresistance (MR) of **1** under the magnetic field along the *b*-axis. The data for 1.3, 0.7, and 0.5 K are shifted upward for clarity. Up- and down-sweep MR are shown in black and gray, respectively.

The spin and charge degrees of freedom are strongly coupled with each other in **1**. The coexistence of AF ordering of *d*-spins and SDW of π-electrons, and their interplay would be essential for the peculiar magnetic and transport properties. It is known that density waves become glassy at low temperatures.[17] We also note that the hysteresis is significantly pronounced only below 1.3 K. A synergistic effect between the glassy nature of SDW and the random exchange is a possible origin for the unconventional hysteresis.

In conclusion, we successfully synthesized mixed-anion π–*d* conductor **1** while keeping the isostructure utilizing iodine bonds. Compound **1** is the first example of a molecular conductor showing a large hysteresis associated with a spin-flop transition in both magnetization and conductivity via strong π–*d* interactions. We also succeeded in tuning the SDW instability and π–*d* interactions by anion mixing. Our results suggest that chemical substitution can cause systematic and drastic changes

in the electronic states, and that iodine-bonded supramolecular systems can be useful to obtain strong correlations. We believe our study will open up the potential of novel physical phenomena and multifunctionality for electronics and spintronics.

Keywords: conducting materials • magnetic properties • organic–inorganic hybrid composites • iodine bonds • random exchange interaction

[1] a) M. N. Baibich, J. M. Broto, A. Fert, F. Nguyen Van Dau, F. Petroff, P. Etienne, G. Creuzet, A. Friederich, J. Chazelas, *Phys. Rev. Lett.* **1988**, *61*, 2472–2475; b) G. Binasch, P. Grünberg, F. Saurenbach, W. Zinn, *Phys. Rev. B* **1989**, *39*, 4828–4830.

[2] a) S. A. Wolf, D. D. Awschalom, R. A. Buhrman, J. M. Daughton, S. von Molnár, M. L. Roukes, A. Y. Chtchelkanova, D. M. Treger, *Science* **2001**, *294*, 1488–1495; b) D. D. Awschalom, M. E. Flatté, *Nat. Phys.* **2007**, *3*, 153–159.

[3] a) M. Chollet, L. Guerin, N. Uchida, S. Fukaya, H. Shimoda, T. Ishikawa, K. Matsuda, T. Hasegawa, A. Ota, H. Yamochi, G. Saito, R. Tazaki, S. Adachi, S. Koshihara, *Science* **2005**, *307*, 86–89; b) F. Sawano, I. Terasaki, H. Mori, T. Mori, M. Watanabe, N. Ikeda, Y. Nogami, Y. Noda, *Nature* **2005**, *437*, 522–524.

[4] a) N. Hanasaki, H. Tajima, M. Matsuda, T. Naito, T. Inabe, *Phys. Rev. B* **2000**, *62*, 5839–5842; b) S. Uji, H. Shinagawa, T. Terashima, T. Yakabe, Y. Terai, M. Tokumoto, A. Kobayashi, H. Tanaka, H. Kobayashi, *Nature* **2001**, *410*, 908–910; c) E. Coronado, J. R. Galán-Mascarós, C. J. Gómez-García, V. N. Laukhin, *Nature* **2000**, *408*, 447–449; d) M. Kurmoo, A. W. Graham, P. Day, S. J. Coles, M. B. Hursthouse, J. L. Caulfield, J. Singleton, F. L. Pratt, W. Hayes, L. Ducasse, P. Guionneaul, *J. Am. Chem. Soc.* **1995**, *117*, 12209–12217; e) H. Kobayashi, H.-B. Cui, A. Kobayashi, *Chem. Rev.* **2004**, *104*, 5265–5288; f) T. Enoki, A. Miyazaki, *Chem. Rev.* **2004**, *104*, 5449–5477; g) *Multifunctional Conducting Molecular Materials* (Eds.: G. Saito, F. Wudl, R. C. Haddon, K. Tanigaki, T. Enoki, H. E. Katz, M. Maesato), RSC Publishing, Cambridge, **2007**; h) *Multifunctional Molecular Materials* (Ed.: L. Ouahab), Pan Stanford Publishing, Singapore, **2013**.

[5] a) K. Enomoto, J. Yamaura, A. Miyazaki, T. Enoki, *Bull. Chem. Soc. Jpn.* **2003**, *76*, 945–959; b) K. Okabe, J. Yamaura, A. Miyazaki, T. Enoki, *J. Phys. Soc. Jpn.* **2005**, *74*, 1508–1520; c) J. Nishijo, A. Miyazaki, T. Enoki, *Inorg. Chem.* **2005**, *44*, 2493–2506; d) T. Enoki, K. Okabe, A. Miyazaki, in *Multifunctional Conducting Molecular Materials* (Eds.: G. Saito, F. Wudl, R. C. Haddon, K. Tanigaki, T. Enoki, H. E. Katz, M. Maesato), RSC Publishing, Cambridge, **2007**, pp. 153–160; e) A. Miyazaki, H. Yamazaki, M. Aimatsu, T. Enoki, R. Watanabe, E. Ogura, Y. Kuwatani, M. Iyoda, *Inorg. Chem.* **2007**, *46*, 3353–3366.

[6] T. Shirahata, M. Kibune, M. Maesato, T. Kawashima, G. Saito, T. Imakubo, *J. Mater. Chem.* **2006**, *16*, 3381–3390.

[7] a) M. Maesato, T. Kawashima, Y. Furushima, G. Saito, H. Kitagawa, T. Shirahata, M. Kibune, T. Imakubo, *J. Am. Chem. Soc.* **2012**, *134*, 17452–17455; b) M. Maesato, T. Kawashima, G. Saito, T. Shirahata, M. Kibune, T. Imakubo, *Phys. Rev. B* **2013**, *87*, 085117.

[8] M. Maesato, Y. Furushima, G. Saito, H. Kitagawa, T. Imakubo, A. Kiswandhi, D. Graf, J. S. Brooks, *J. Phys. Soc. Jpn.* **2013**, *82*, 043704.

[9] An iodine bond is the strongest halogen bonds; a) T. Imakubo, H. Sawa, R. Kato, *Synth. Met.* **1995**, *73*, 117–122; b) T. Imakubo, N. Tajima, M. Tamura, R. Kato, Y. Nishio, K. Kajita, *J. Mater. Chem.* **2002**, *12*, 159–161; c) M. Fourmigué, P. Batail, *Chem. Rev.* **2004**, *104*, 5379–5418; d) P. Metrangolo, F. Meyer, T. Pilati, G. Resnati, G. Terraneo, *Angew. Chem. Int. Ed.* **2008**, *47*, 6114–6127; *Angew. Chem.* **2008**, *120*, 6206–6220; e) P. Politzer, J. S. Murray, *ChemPhysChem* **2013**, *14*, 278–294; f) T. Imakubo, M. Kobayashi, *Eur. J. Inorg. Chem.* **2014**, *24*, 3973–3981.

[10] a) T. Imakubo, T. Shirahata, *Chem. Commun.* **2003**, 1940–1941; b) T. Imakubo, T. Shirahata, M. Kibune, H. Yoshino, *Eur. J. Inorg. Chem.* **2007**, 4727–4735.

[11] B. R. McGarvey, M. J. Taylor, D. G. Tuck, *Inorg. Chem.* **1981**, *20*, 2010–2013.

[12] CCDC 1054133 [**1**] and 1054132 [**2**] contain the supplementary crystallographic data for this paper. These data can be obtained free of charge from The Cambridge Crystallographic Data Centre via www.ccdc.cam.ac.uk/data_request/cif.

[13] C. Michioka, Y. Itoh, K. Yoshimura, T. Furushima, M. Maesato, G. Saito, T. Shirahata, M. Kibune, T. Imakubo, *J. Phys.: Conf. Ser.* **2009**, *150*, 042124.

[14] M. Enomoto, A. Miyazaki, T. Enoki, *Mol. Cryst. Liq. Cryst.* **1999**, *335*, 293–302.

[15] a) B. Zhang, Z. Wang, Y. Zhang, K. Takahashi, Y. Okano, H.-B. Cui, H. Kobayashi, K. Inoue, M. Kurmoo, F. L. Pratt, D. Zhu, *Inorg. Chem.* **2006**, *45*, 3275–3280; b) T. Hayashi, X. Xiao, H. Fujiwara, T. Sugimoto, H. Nakazumi, S. Noguchi, H. Aruga-Katori, *Inorg. Chem.* **2007**, *46*, 8478–8480.

[16] a) A. Paduan-Filho, C. C. Becerra, F. Palacio, *Phys. Rev. B* **1991**, *43*, 11107–11111; b) C. C. Becerra, A. Paduan-Filho, F. Palacio, V. B. Barbeta, *J. Appl. Phys*. **1993**, *73*, 5491–5493.

[17] a) G. Grüner, *Rev. Mod. Phys.* **1988**, *60*, 1129–1181; b) P. Monceau, *Adv. Phys*. **2012**, *61*, 325–581.

Entry for the Table of Contents

COMMUNICATION

Blend halogens: A radical cation salt was synthesized using halogen-mixed magnetic anions. The crystal structure is robust against random halogen substitution due to iodine bonds. The material shows unprecedented hysteresis in both magnetic moment and magnetoresistance associated with a spin-flop transition.

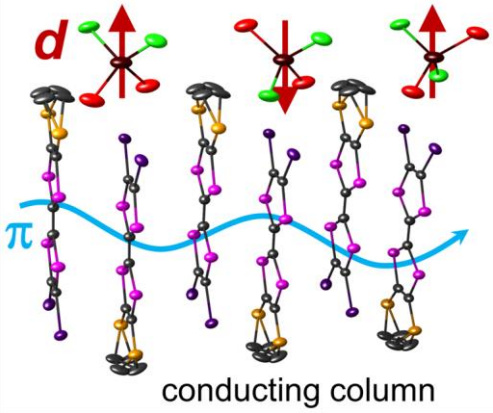

Genta Kawaguchi, Mitsuhiko Maesato, Tokutaro Komatsu, Hiroshi Kitagawa, Tatsuro Imakubo, Andhika Kiswandhi, David Graf, and James S. Brooks*

Page No. – Page No.

Unconventional Magnetic and Resistive Hysteresis in an Iodine-Bonded Molecular Conductor

Contents

1. Elemental analysis by EDX techniques

To confirm the composition of Br and Cl, EDX measurements were performed using JEOL JSM5510/JED2210 in the Research Center for Low Temperature and Materials Sciences, Kyoto University, Japan. Table S1 shows the average stoichiometry determined from the EDX data, which is consistent with the synthetic ratio.

Table S1. Br/Cl ratio estimated from EDX data

Sample	Synthetic Br/Cl ratio	Observed Br/Cl ratio
$(DIETSe)_2FeBr_2Cl_2$	50/50	51(2)/49(2)
$(DIETSe)_2GaBr_2Cl_2$	50/50	48(2)/52(2)

2. Crystal structure analysis of $(DIETSe)_2MBr_2Cl_2$ [M = Fe, Ga]

Single crystal X-ray diffraction data were collected using a Bruker SMART APEX II ULTRA CCD diffractometer employing graphite-monochromated Mo *K*α radiation at 293 K. A single crystal of $(DIETSe)_2MBr_2Cl_2$ [M = Fe, Ga] was mounted on a glass fiber. The crystal structures were solved using a direct method (SIR2011)[S1] and refined on F^2 using a full-matrix least-squares method with the SHELXL2013.[S2] All calculations were performed using the CrystalStructure software package.[S3] Crystallographic data in CIF format have been deposited in the Cambridge Crystallographic Data Centre (CCDC) under deposition numbers CCDC 1054132, 1054133.

Table S2. Crystallographic data of $(DIETSe)_2MBr_2Cl_2$ [M = Fe, Ga]

Compounds	**$(DIETSe)_2FeBr_2Cl_2$**	**$(DIETSe)_2GaBr_2Cl_2$**
Formula	$C_{16}H_8I_4S_4Se_8FeBr_2Cl_2$	$C_{16}H_8I_4S_4Se_8GaBr_2Cl_2$
Formula weight	1754.34	1768.18
Temperature	293 K	293 K
Crystal size	$0.27 \times 0.08 \times 0.01$ mm^3	$0.18 \times 0.16 \times 0.02$ mm^3
Crystal system	Orthorhombic	Orthorhombic
Space group	*Ibam* (#72)	*Ibam* (#72)
a	7.3328(6) Å	7.3400(7) Å
b	36.365(3) Å	36.3615(3) Å
c	13.5901(12) Å	13.5970(13) Å
α	90º	90º
β	90º	90º
γ	90º	90º
V	3623.9(5) Å^3	3628.9(6) Å^3
Z	4	4
Density (calcd)	3.215 g/cm^3	3.236 g/cm^3
F(000)	3128	3148
μ(Mo *K*α)	14.465 mm^{-1}	14.787 mm^{-1}
Abs. correction	Multi-scan	Multi-scan
Reflections collected	9844	9817
Reflections unique	2250	2244
R_{int}	0.0403	0.0351
R_1 (I>2σ(I))	0.0360	0.0246
wR_2 (all data)	0.0999	0.0762
Goodness-of-fit (GOF)	1.119	1.106
Residual electron density max/min	0.698/–0.893 e Å^{-3}	0.564/–0.670 e Å^{-3}

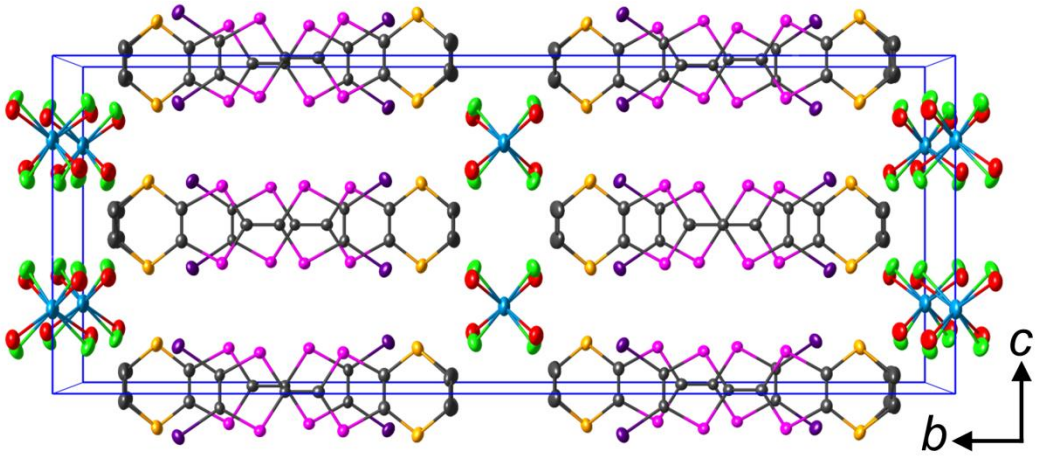

Figure S1. Crystal structure of $(DIETSe)_2GaBr_2Cl_2$ viewed along the *a*-axis. C, I, Se, S, Ga, Br, and Cl atoms are shown in gray, violet, pink, yellow, light blue, red, and green, respectively, using a thermal ellipsoid model (50% probability). The site occupancy factors of Br and Cl are 0.5.

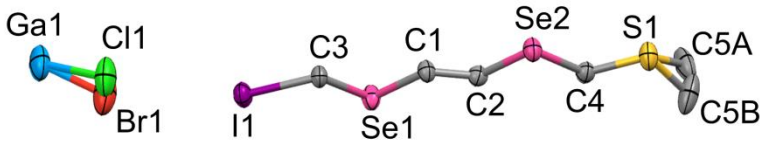

Figure S2. Asymmetric unit of $(DIETSe)_2GaBr_2Cl_2$ (thermal ellipsoid, 50% probability). The $FeBr_2Cl_2$ salt has an equivalent asymmetric unit.

Specific refinement details

As shown in Figure S2, the residual electron density map suggested two crystallographically independent halide anion (Br^-, Cl^-) sites, which form tetrahedral anion ($MBr_2Cl_2^-$, M = Fe, Ga) units in the unit cell. Considering the results of the EDX analysis (Table S1), we determined the positions of the halide anion species (Br^-, Cl^-) with fixed site occupancies (0.5 for each) in the refinement process. The site occupancies of the carbon atoms in the ethylene groups (C5A and C5B) were also fixed (0.5 for each).

3. Band calculations

Band calculations were carried out using density functional theory (PBE functional)[S4] implemented in CASTEP[S5] in Materials Studio (Accelrys Software Inc.). Plane-wave basis functions with a cutoff energy of 330 eV were used with ultrasoft pseudopotentials.[S6] The hydrogen atoms of the ethylene groups in the $FeBr_2Cl_2$ and $GaBr_2Cl_2$ salts were attached assuming a C–H bond distance of 1.07 Å and sp^3 hybridization. The reported crystal structures[S7] were used for the pristine compounds. To eliminate the disorder in the ethylene groups, the symmetry of the crystal was lowered from Ibam (D2h) to I2/b (C2h), Pbcn (D2h), Pccn (D2h), and I222 (D2). The relative energies in the case of the $GaCl_4$ salt were 1.8, 0.0, 4.4, and 2.0 meV, respectively. The Fermi surfaces were obtained for the lowest energy conformation, Pbcn. The calculated Fermi surfaces of the MCl_4, MBr_2Cl_2, MBr_4 [M = Fe, Ga] salts are almost identical, with a Fermi pocket whose area is 9–10% of the first Brillouin zone (FBZ). Even though the Fermi surfaces of the pristine salts calculated using the extended Hückel method[S8] indicated a pocket with an area of ca. 5% of the FBZ,[S7] we observed quantum oscillations in magnetoresistance corresponding to an area of about 10% in some of the pristine and mixed salts,[S9] supporting the DFT calculations.

4. Methods of physical property measurements

The magnetic susceptibility of $(DIETSe)_2FeBr_2Cl_2$ was measured using Quantum Design SQUID magnetometers (MPMS-XL5, MPMS-XL7) and a ^{3}He gas handling system (IQUANTUM iHelium3) in the Research Center for Low Temperature and Materials Sciences, Kyoto University, Japan. The single crystals were arranged on Cu plate using a small amount of Apiezon N grease so that all the crystals were aligned in the same direction. The contributions of the sample holder were subtracted by blank experiments, except for the experiments using ^{3}He. The diamagnetic susceptibility of the DIETSe molecule was evaluated to be -2.46×10^{-4} emu/mol, as previously reported.[S7] The core diamagnetic susceptibility of the $FeBr_2Cl_2^-$ anion was estimated using Pascal's table to be -1.34×10^{-4} emu/mol.

The electrical resistivity of the MBr_2Cl_2 and MX_4 [M = Fe, Ga; X = Cl, Br] salts was measured along the least conducting *b*-axis using a four-probe dc method. Four gold wires (10 μm in diameter) were attached to a single crystal with carbon paste as the electrodes. To prevent cracks forming during cooling, a moderate hydrostatic pressure (< 1.5 kbar) was applied to the crystal at room temperature using a BeCu piston–cylinder-type pressure cell. Daphne 7373 was used as the pressure medium. The pressure loss during cooling has been reported to be ca. 1.5 kbar.[S10] We also confirmed that at low temperatures the pressure was almost the same as ambient pressure by monitoring the superconducting transition temperature of tin. The resistivity was measured down to 0.5 K using a ^{3}He cryostat. The magnetoresistance of the MBr_2Cl_2 [M = Fe, Ga] salts was measured under magnetic field applied parallel to the *b*-axis. A solenoid-type superconducting magnet was used to generate magnetic fields up to 12 T.

The magnetic torque of a single crystal of the $FeBr_2Cl_2$ salt was measured using a piezoresistive microcantilever for atomic force microscopy. Employing a Wheatstone bridge circuit, the torque difference between the sample and reference cantilevers was read out.[S11] Strong magnetic fields up to 35 T were applied along the *b*-axis using a dc resistive magnet at the National High Magnetic Field Laboratory (NHMFL), USA.

5. Resistivities of $(DIETSe)_2GaCl_4$, $(DIETSe)_2GaBr_2Cl_2$, and $(DIETSe)_2GaBr_4$

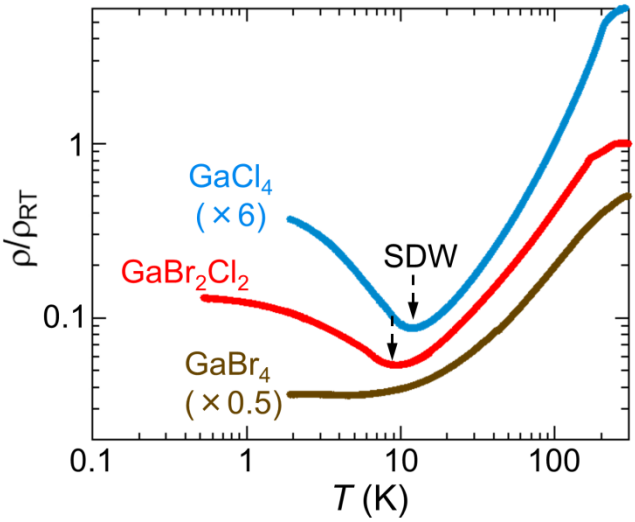

Figure S3. Electrical resistivity along the *b*-axis of the $GaCl_4$, $GaBr_2Cl_2$, and $GaBr_4$ salts, normalized by the value at 300 K. For clarity, the values of the $GaCl_4$ and $GaBr_4$ salts are multiplied by 6 and 0.5, respectively. Broken arrows show SDW transitions.

6. Curie–Weiss fitting of $(DIETSe)_2FeBr_2Cl_2$

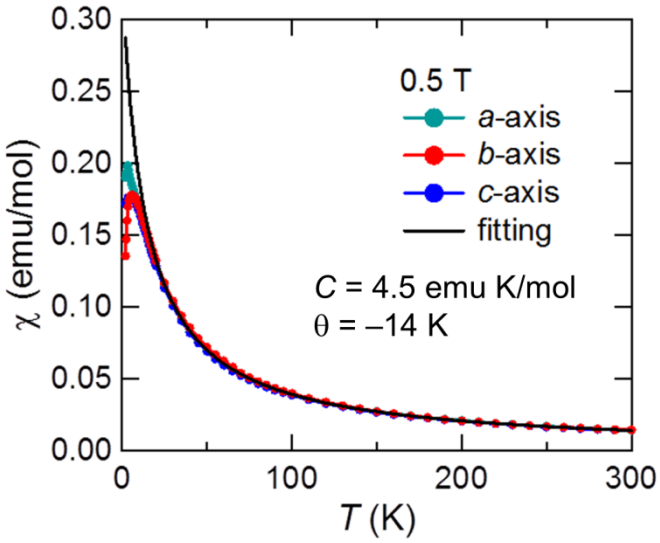

Figure S4. Temperature dependence of the magnetic susceptibility of $(DIETSe)_2FeBr_2Cl_2$ at 0.5 T. The core diamagnetic susceptibility is already subtracted. As shown by the black line, the susceptibility is well fitted by the Curie–Weiss law with Curie constant C = 4.5 emu K/mol and Weiss temperature θ = –14 K above 20 K. Obtained C is consistent with Fe^{3+} spins (S = 5/2, C = 4.4 emu K/mol). Negative θ indicates an antiferromagnetic interaction.

7. Magnetization hysteresis in $(DIETSe)_2FeBr_2Cl_2$

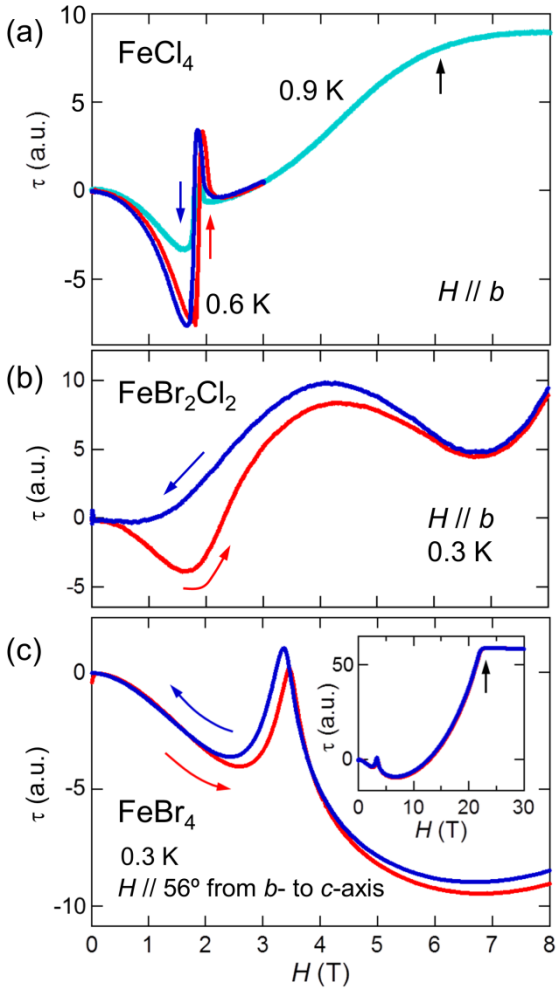

Figure S5. Magnetic field dependence of the magnetic torque of the (a) $FeCl_4$, (b) $FeBr_2Cl_2$, and (c) $FeBr_4$ salts at very low temperatures (< 1 K). The magnetic field direction is near to the easy axis for each salt.[S12–14] Red and blue curves represent up- and down-sweep magnetic torque. Black arrows in (a) and inset of (c) show the saturation fields of the $FeCl_4$ and $FeBr_4$ salts are 6 and 22 T, respectively. The $FeCl_4$ and $FeBr_4$ salts show marked changes in torque from spin-flop transitions, accompanied by a very small hysteresis. In contrast, the $FeBr_2Cl_2$ salt displays an extraordinarily large hysteresis in torque around the spin-flop transition, strongly suggesting an anion mixing effect.

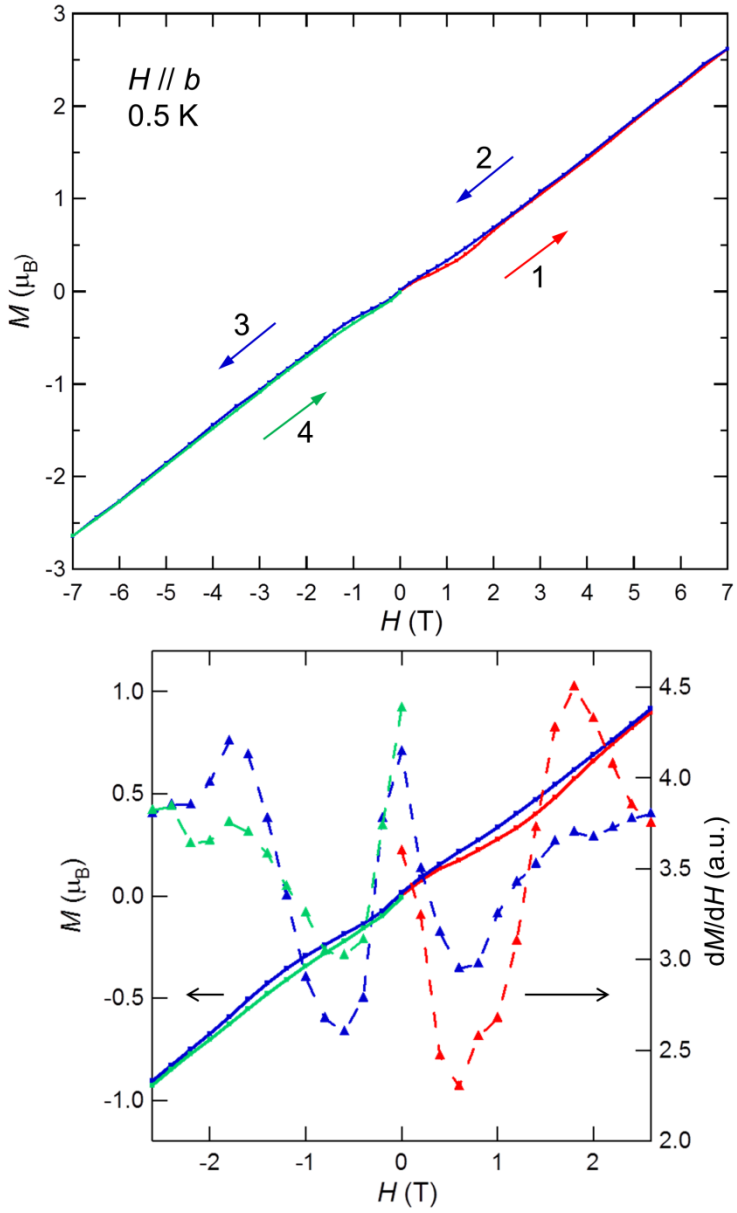

Figure S6. Magnetic field dependence of the magnetization of the $FeBr_2Cl_2$ salt at 0.5 K including the negative field range. Lower figure shows an extended region of the upper figure. Solid and dashed lines represent the magnetization M (left axis) and dM/dH (right axis), respectively. Line colors indicate successive field sweeping as follows; red: 0 → 7 T, blue: 7 → 0 → –7 T, green: –7 → 0 T.

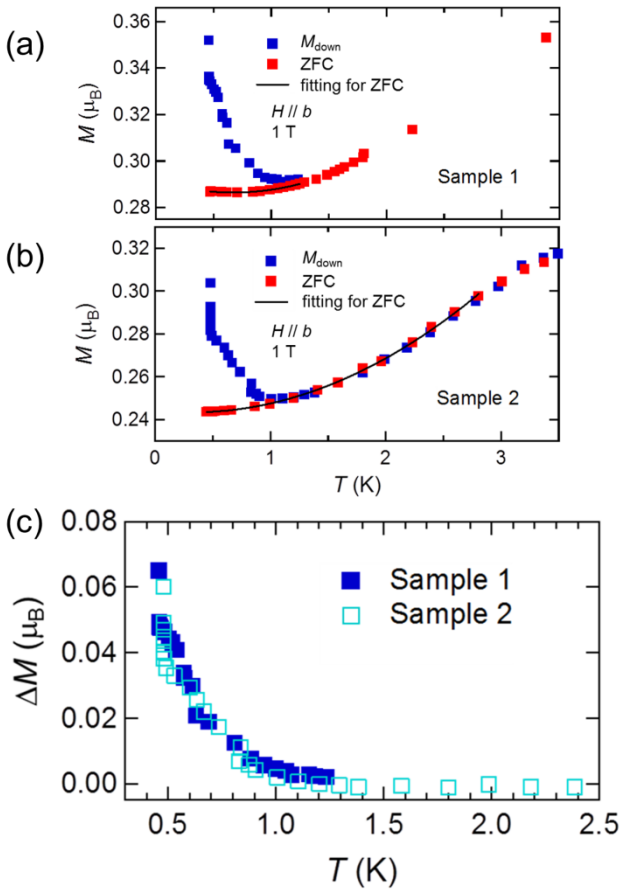

Figure S7. Temperature dependence of the magnetization for two samples (a, b) for two different processes: (i) ZFC (red squares) and (ii) heating from the field-induced state (blue squares). In process (i), the sample was first cooled to 0.5 K at 0 T, and then a field of 1 T was applied and the magnetization was measured at 1 T on heating. In process (ii), the sample was cooled to 0.5 K at 0 T, and then the magnetic field was increased to 5 T to induce a spin-flop transition. Then, the field was decreased to 1 T and the magnetization was measured at 1 T. Black line shows the fitting for the ZFC data. (c) Difference in the magnetization obtained by subtracting the fit of the ZFC data from the M_{down} data for two different samples, indicating a good reproducibility.

8. Spin–charge coupling in $(DIETSe)_2FeBr_2Cl_2$

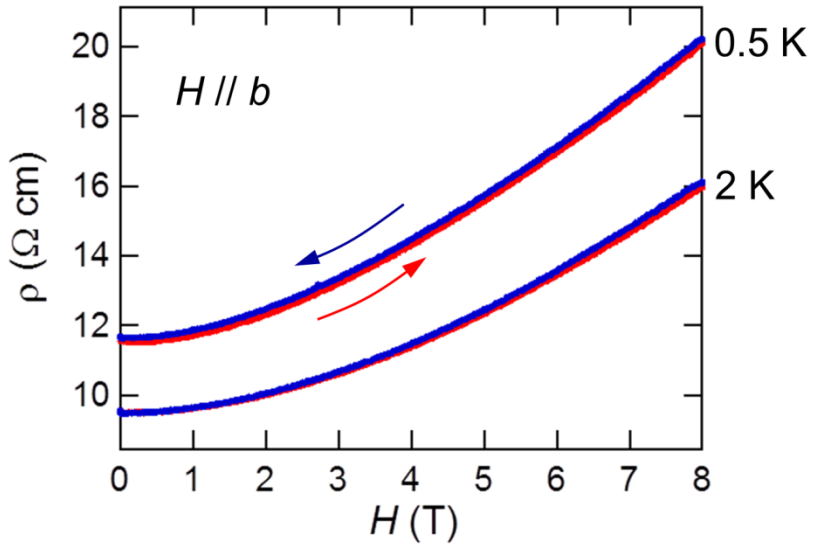

Figure S8. MR of the nonmagnetic $GaBr_2Cl_2$ salt. Up- and down-sweep MR are colored red and blue, respectively. MR increases monotonically with increasing magnetic field.

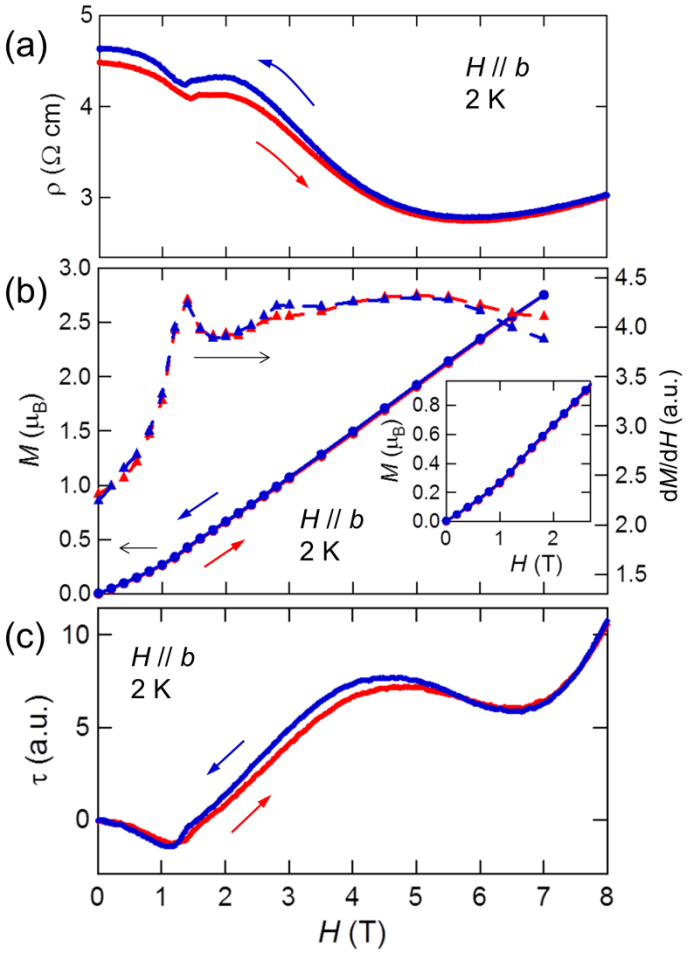

Figure S9. Comparison of (a) MR, (b) magnetic moment *M*, and (c) magnetic torque τ, of the $FeBr_2Cl_2$ salt at 2 K. Magnetic field was applied along the *b*-axis, corresponding to the magnetic easy axis. The inset of (b) shows an extended region of *M*. Dip structure in the MR at 1.4 T is confirmed to correspond to a spin-flop transition since the peak in the derivative of the magnetization d*M*/d*H* and a steep increase in τ are clearly observed. MR shows hysteresis involving a change in the zero-field resistance before and after the spin-flop, while *M* and τ show negligible or only a small hysteresis. These results are similar to the mother compound, $(DIETSe)_2FeCl_4$.[S12]

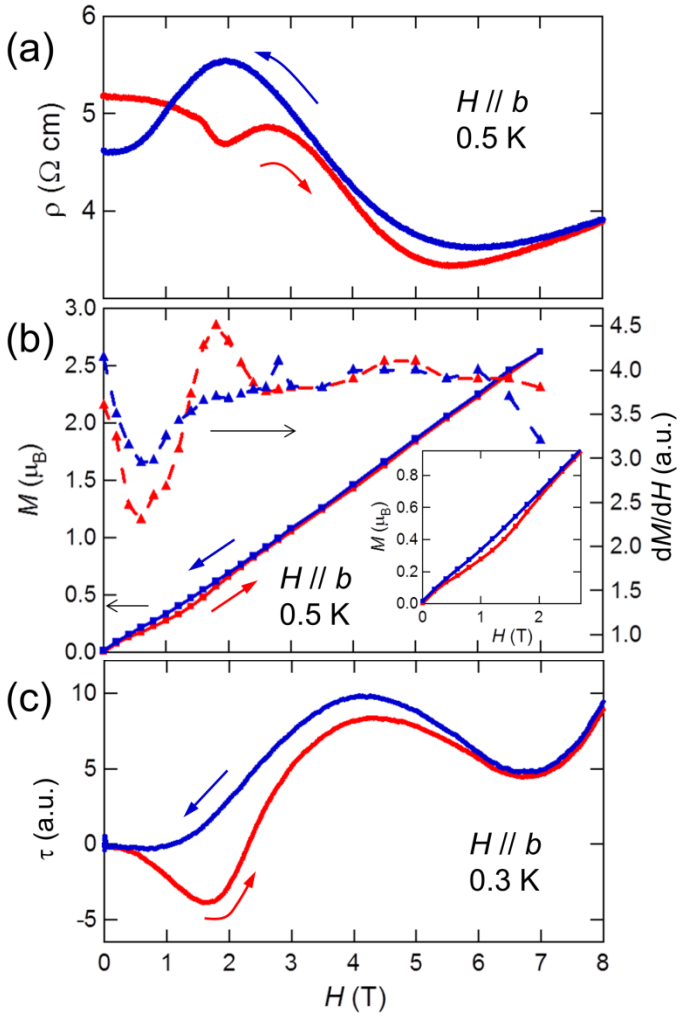

Figure S10. Comparison of (a) MR, (b) magnetic moment *M*, and (c) magnetic torque τ, of the $FeBr_2Cl_2$ salt at 0.5, 0.5, and 0.3 K, respectively. Magnetic field was applied along the *b*-axis corresponding to the magnetic easy axis. The inset of (b) shows an extended region of *M*. These figures show well-correlated magnetic and transport behaviors with a large hysteresis at spin-flop transition. At very low temperatures, a clear, significant hysteresis appears in the MR but also in the *M* and τ curves, in marked contrast to the very small hysteresis at 2 K (Figure S9). It should be noted that the features of the spin-flop transition are clear in the MR, *M*, and τ curves in the up-sweep, while they are not clear in the down-sweep. This suggests successive changes in the ratio of AF and CAF domains in the down-sweep.

References

[S1] M. C. Burla, R. Caliandro, M. Camalli, B. Carrozzini, G. L. Cascarano, C. Giacovazzo, M. Mallamo, A. Mazzone, G. Polidori, R. Spagna, *J. Appl. Crystallogr.* **2012**, *45*, 357–361.

[S2] G. M. Sheldrick, *Acta. Crystallogr.* **2008**, *A64*, 112–122.

[S3] CrystalStructure 4.1: Crystal Structure Analysis Package, Rigaku Corporation, Japan (2000–2014).

[S4] J. P. Perdew, K. Burke, M. Ernzerhof, *Phys. Rev. Lett.* **1996**, *77*, 3865–3868.

[S5] S. J. Clark, M. D. Segall, C. J. Pickard, P. J. Hasnip, M. J. Probert, K. Refson, M. C. Payne, *Zeitschrift fur Kristallographie* **2005**, *220*, 567–570.

[S6] D. Vanderbilt, *Phys. Rev. B* **1990**, *41*, 7892–7895.

[S7] T. Shirahata, M. Kibune, M. Maesato, T. Kawashima, G. Saito, T. Imakubo, *J. Mater. Chem.* **2006**, *16*, 3381–3390.

[S8] T. Mori, A. Kobayashi, Y. Sasaki, H. Kobayashi, G. Saito, H. Inokuchi, *Bull. Chem. Soc. Jpn.* **1984**, *57*, 627–633.

[S9] To be reported elsewhere.

[S10] K. Murata, H. Yoshino, H. O. Yadav, Y. Honda, N. Shirakawa, *Rev. Sci. Instrum.* **1997**, *68*, 2490–2493.

[S11] E. Ohmichi, T. Osada, *Rev. Sci. Instrum.* **2002**, *73*, 3022–3026.

[S12] M. Maesato, T. Kawashima, Y. Furushima, G. Saito, H. Kitagawa, T. Shirahata, M. Kibune, T. Imakubo, *J. Am. Chem. Soc.* **2012**, *134*, 17452–17455.

[S13] M. Maesato, T. Kawashima, G. Saito, T. Shirahata, M. Kibune, T. Imakubo, *Phys. Rev. B* **2013**, *87*, 085117.

[S14] M. Maesato, Y. Furushima, G. Saito, H. Kitagawa, T. Imakubo, A. Kiswandhi, D. Graf, J. S. Brooks, *J. Phys. Soc. Jpn.* **2013**, *82*, 043704.